Lab on a Chip

Muscle-on-a-chip with on-site multiplexed biosensing system for in situ-monitoring of secreted IL-6 and TNF-α

Journal:	*Lab on a Chip*
Manuscript ID	LC-ART-03-2019-000285.R2
Article Type:	Paper
Date Submitted by the Author:	16-Jun-2019
Complete List of Authors:	Ortega Machuca, Maria; Institute for Bioengineering in Catalunya, Biosensors for Bioengineering Fernández Garibay, Xiomara; Institute for Bioengineering in Catalunya, Biosensors for Bioengineering G. Castaño, Albert; Institute for Bioengineering in Catalunya Chiara, Francesco ; Institute for Bioengineering in Catalunya, Biosensors for Bioengineering Hernandez Albors, Alejandro; Institute for Bioengineering in Catalunya, Biosensors for Bioengineering Balaguer Trias, Jordina; Institute for Bioengineering in Catalunya, Biosesnors for Bioengineering Ramon Azcon, Javier; Institute for Bioengineering in Catalunya, Biosensors for Bioengineering

ARTICLE

Muscle-on-a-chip with on-site multiplexed biosensing system for in situ-monitoring of secreted IL-6 and TNF-α

Received 00th January 20xx,
Accepted 00th January 20xx

DOI: 10.1039/x0xx00000x

María A. Ortega[a], Xiomara Fernández-Garibay[a], Albert G. Castaño[a], Francesco De Chiara[a], Alejandro Hernández-Albors [a], Jordina Balaguer-Trias [a] and Javier Ramón-Azcón [a]

Despite the increasing number of organs-on-a-chip that have been developed in the last decade, limited efforts have been made to integrate a sensing system for in-situ continual measurements of biomarkers from three-dimensional (3D) tissues. Here, we present a custom-made integrated platform for muscle cell stimulation under fluidic conditions connected with a multiplexed high-sensitive electrochemical sensing system for in-situ monitoring. To demonstrate this, we use our system to measure the release levels and released time of interleukin 6 and tumor necrosis factor alpha in vitro by 3D muscle microtissue under electrical and biological stimulations. Our experimental design has enabled us to perform multiple timepoint measurements using functionalized screen-printed gold electrodes with a sensitivity in the ng mL^{-1} range. This affordable set up is uniquely suited for monitoring factors released by 3D single cell type upon external stimulation for metabolic studies

1. Introduction

In vitro biomimetic tissue models with physiological functions can be used to assess biological phenomena in an easy, accurate, and controllable manner. Current in vitro tissues are useful for studying both the molecular and the cellular bases of physiological and pathological responses of biological processes. To this end, microscale fabrication technologies have emerged as useful tools in tissue engineering and biological applications.[1] Further, these models promise to replace corresponding animal experiments, which are costly, labor-intensive, and beset with serious ethical issues regarding their biological relevance to humans.[2]

In addition, almost 40% of total body mass is skeletal muscle (SM) tissue. Although people associate it with strength and movement, its functions range from controlling facial expressions to helping respiratory and blood circulation. The skeletal muscle tissue contains numerous quiescent mononucleate satellite cells which undergo to intense proliferation after tissue damage to self-repair. This capacity is impaired or even lost in patients with congenital defects, diabetes, cancer and/or after traumatic injuries and protracted denervation.[3] According to the American Medical Association, there is no specialized clinical doctor for the treatment of muscular diseases, such as Duchenne muscular dystrophy and inflammatory myopathy, hence the necessity to fill the gap between the muscle disorders and ad hoc therapies is highly desirable. Moreover, none or too little knowledge is present about the source and auto-paracrine impact of cytokine release such as IL-6 and TNF-α in tissue regeneration. To this end, tissue engineering represents a fascinating and affordable approach to shed light on understanding the mechanisms and actors involved in the development of muscular disease.

Besides, in the field of biomimetic tissues, the need to incorporate biosensing for in-situ monitoring of the status or the secretion regimes of in vitro microtissues is increasingly recognized.[4, 5] Additionally, the capability to miniaturize biosensor systems and advanced tissue fabrication procedures have enabled researchers to create multiple tissues on a chip with a high degree of control over experimental variables for high-content screening applications.[6] While recent organs-on-a-chip (OOCs) can model native-organ microstructures for understanding disease mechanisms, current OOCs still lack the precise temporal control needed to study processes such as delayed cell response to treatment and chronic effects caused by long-term drug stimulation. Specifically, the difficulty arises when integrating the capability of stimulating the cells of interest with the capability of monitoring individual analytes released in-situ. For example, OCCs that utilize magnetic particles,[7] or impedimetric sensors[2, 4, 5] to facilitate analyte detection, are either time-sensitive, or unstable under changing medium composition.

Here, we present a cost-effective integrated microdevice capable of simultaneous, in-situ cell stimulation and analyte detection that is stable over time. We demonstrate this using a microdevice that targets 3D skeletal-muscle tissue, known to release cytokines under external stimulations. With this setup, we can provide either electrical stimulation using indium tin oxide (ITO)-interdigitated arrays (IDA) electrodes, or biological stimulation using lipopolysaccharide (LPS) solutions. Simultaneously, we can achieve multiplexed continual in-situ measurements of secreted myokines using functionalized high-sensitive screen-printed gold electrodes

[a] Institute for Bioengineering of Catalonia (IBEC), The Barcelona Institute of Science and Technology (BIST). Baldiri I Reixac, 10-12, 08028, Barcelona, Spain.
Email: jramon@ibecbarcelona.eu
†Electronic Supplementary Information (ESI) available: See DOI: 10.1039/x0xx00000x

(SPGEs) (Fig. 1). Our setup demonstrates that microfluidics combined with tissue engineering and biosensing is an affordable approach in determining the response upon external stimuli. This device can be involved in the study of various muscular-diseases progression, furthering the understanding and treatment of muscular metabolic disorders

2. Materials and Methods

2.1 Cell culture

Murine C2C12 skeletal myoblasts (CRL-1772, ATCC, Virginia, USA) were expanded in growth medium, which consisted of Dulbecco's Modified Eagle Medium (DMEM high glucose, L-glutamine) (11965092, Gibco, Thermofisher, Massachusetts, USA) supplemented with fetal bovine serum (10%, FBS) (16000044, Thermofisher, Massachusetts, USA) and penicillin/streptomycin (1%) (15140122, Thermofisher, Massachusetts, USA) at 37 ºC and 5% CO2 atmosphere. To induce differentiation into myotubes, the medium was changed to a differentiation medium, based in DMEM high glucose, supplemented with horse serum (2%) (HS) (26050088, Thermofisher, Massachusetts, USA) and 1% penicillin/streptomycin.

2.2 Synthesis of prepolymer precursors

Gelatin methacryloyl (GelMA) was synthesized with a 40% degree of methacrylation as previously described.[8] The material was then dialyzed in Milli Q water with 6-8 kDa MWCO membranes (08-700-142, Spectrumlabs, San Francisco, USA) for 4 days. Sodium carboxymethylcellulose (CMC) (419273, Sigma Aldrich Co. St Louis. MO, USA) was methacrylated at a maximum degree of methacrylation as previously described.[8] The reaction was performed by mixing a solution of the polymer (1% w/v) in MES buffer (50mM, pH 6.5) with a mix of EDC (20mM), N-hydroxysuccinimide (10mM) (130672, Sigma Aldrich Co. St Louis. MO, USA) and 2 aminoethylmethacrylate (10 mM) (479659, Sigma Aldrich Co. St Louis. MO, USA). The reaction was stopped after 24 h with the addition of acetone (161007, Panreac, Barcelona, Spain) and filtered using a vacuum flask. The precipitate was dissolved in PBS (10 mM) and dialyzed in Milli Q water with 3.5 kDa MWCO membranes (68035, Thermofisher, Massachusetts, USA). Finally, the solutions of methacrylated polymers (GelMA and CMCMA) were lyophilized and stored at -20 ºC.

2.3 Preparation of prepolymer solutions

The prepolymer precursors (GelMA and CMCMA) were dissolved in growth medium, containing the photoinitiator lithium Phenyl (2,4,6-trimethylbenzoyl) phosphinate (LAP) (L0290, TCI EUROPE N.V, Zwijndrecht, Belgium), at 65 ºC for 3 h to obtain a homogeneous solution. The concentrations of GelMA, CMCMA and LAP were fixed to obtain final concentrations of 5%, 1% and 0.1% (w/v), respectively.

2.4 Hydrogel characterization

2.4.1 Swelling analysis. The prepolymer solutions were prepared as described above. Samples for swelling analysis were fabricated by placing the prepolymer solution (300 µL) in a 48 well-plate. After exposing the prepolymer solution to UV light (UVP Crosslinker, Model CL-1000L, 365 nm, 40W, from Analytik Jena US, Upland, USA), hydrogels were rinsed with PBS and their initial weight was measured. Then, the wet weight was determined after 1, 3, and 7 days in PBS (10 mM), after a wipe with tissue paper to remove the excess water. To calculate the mass increase, each water content value was normalized with the initial weight of the sample. After day 7 samples were rinsed with Milli-Q water and dried. The swelling ratio, Q, of the hydrogels was determined by

$$\boldsymbol{Q = \frac{W_s - W_d}{w_d} x 100} \quad (1)$$

Here, W_d and W_s represent the weight of dried hydrogels and the weight after swelling in PBS, respectively.

2.4.2 Mechanical analysis. Uniaxial compression tests of hydrogels were performed using a Zwick Z0.5 TN instrument (058993, Zwick-Roell, Berlin, Germany) with a 5 N load cell. Hydrogels were fabricated following the same procedure as for the swelling analysis. After reaching equilibrium swelling in PBS, cylindrical hydrogels were cut using a 10 mm diameter biopsy punch. Real hydrogel diameters and heights were measured prior to the experiment. Wet samples were tested at room temperature up to 30% final strain (deformation), using the following parameters: 0.1 mN preload force and 20% min^{-1} strain rate. Stress-strain data was obtained from force-deformation graphs (Fig. S2A†). Values for the compressive modulus were calculated from the slope of the linear region corresponding to 10-20% strain. With uniaxial compressive testing, the software (Zwick Roell, TestXPert software) converts the load-deformation data to stress-strain data using simple geometrical relationships (from measured hydrogel disks), and the Young's modulus E is reported.[9] For each hydrogel formulation, three samples were prepared, and measurements were performed in triplicate.

2.4.3 Degradation analysis. Hydrogels were fabricated as described above for the swelling analysis. Hydrogels were removed from the 48 well-plate and left swelling for 3 days in a 6 well-plate. A total of 3 mL of collagenase type II (0.5 U mL^{-1}) (17101015, Thermofisher, Massachusetts, USA) in PBS was added on the hydrogels and they were incubated at 37ºC, under 100 rpm shaking conditions. Then, hydrogels were weighted after 1, 2, 3, 4, and 4 h. The percent hydrogel remaining (W_r) was determined by:

$$\%\boldsymbol{W_r = \frac{W_t}{W_i} x 100} \quad (2)$$

Here, W_t and W_i represents the weight of hydrogel composites at the swelling equilibrium and after collagenase incubation respectively.

2.5. Cell encapsulation in 3D micropatterns

To encapsulate the cells in micropatterns photomold patterning techniques was used.[10] For that, one volume of prepolymer solution was mixed with one volume of C2C12 cell suspension to obtain a final cell density of 2.5 x 10^7 cells mL^{-1}. Then, a drop of cell-laden prepolymer (15 µL) was placed in the bioreactor well, and a micro-structured PDMS stamp of 6mm in diameter (Fig. 4A), was pressed lightly on top (grooves of 200 µm and 270 µm in height, and ridges of 200 µm, with a length of 5mm approximately), filling the microchannels with the solution. The hydrogel was photo-crosslinked using a UVP Crosslinker (Model CL-1000L, 365 nm, 40W, from Analytik Jena US, Upland, USA) with exposure times between 18 s and 120 s. Energy dose for every time point was measured using a wireless powermeter (model PM160 Si Sensor Power Meter with Bluetooth and USB Operation, 400 - 1100 nm, 10 nW - 200 mW, Thorlabs, CA, USA). After carefully removing the stamp, the microdevice was sealed with a cover glass slide. The micro-structured cell-laden hydrogels were incubated inside the microdevice with growth medium for 6 days. After, the culture medium was switched to differentiation medium (DM) to promote the formation of myotubes. All subsequent experiments were performed in DM cell medium.

2.6. C2C12 morphology and viability in composite hydrogels

C2C12 cells were encapsulated in GelMA-CMCMA hydrogels at a low cell density (1 x 10^6 cells/mL) using protocol previously described.[8] Bright-field microscopy images obtained after 6 days of encapsulation were analyzed using ImageJ software to obtain cell descriptor data of aspect ratio and circularity of cells encapsulated in composite hydrogels with different exposure times. Cell viability was evaluated after 1, 6 and 10 days using the Live/Dead Viability/Citotoxicity assay kit (L3224, Thermofisher, Massachusetts, USA). Confocal microscopy images were obtained and processed by a custom MATLAB software code used in our previous work.[8] Cell viability percentage was calculated as the fraction of living cells over the total cell number.

2.7. Immunofluorescence staining

The tissues were fixed in a formalin solution (10%) (HT501128, Sigma Aldrich Co. St Louis. MO, USA) 15 days after fabrication. Then hydrogels were washed with tris-buffered saline (TBS, BR0042, Canvax Biotech, Spain). Cells were permeabilized with Triton X-100 (0.1%) (X100, Sigma Aldrich Co. St Louis. MO, USA) in TBS for 15 min and blocked with a blocking buffer consisting of Triton X-100 (0.3%) and donkey serum (3%) (D9663, Sigma Aldrich Co. St Louis. MO, USA) in TBS for 2 h. Afterwards, tissues were washed with TBS and incubated in Rhodamine-Phalloidin 480 (100 nM) (PHDR1, Cytoskeleton Inc, Colorado, USA) solution overnight to stain filamentous actin (F-actin). An additional overnight staining for Myosin Heavy Chain (MHC) was performed by incubating in a solution of MF20 Alexa Fluor 488 (5 µg mL^{-1}) (53-6503-82, eBioscience, Thermofisher, Massachusetts, USA) in blocking buffer. After washing with TBS, nuclei were counterstained with DAPI (1 µM, D1306, Thermofisher, Massachusetts, USA) for 15 min. Hydrogels were mounted and stored at 4 ºC before observation by confocal microscopy.

2.8. Microdevice fabrication

2.8.1 ITO-IDA electrodes fabrication. Indium tin oxide (ITO) on glass substrates were commercial (CEC020S, 100 nm thickness, 20 Ohms sq-1, Präzisions Glas & Optik, Iserlohn, Germany), with dimensions of 60 x 60 x 1.1 mm for large, width and thickness respectively. The interdigitated electrodes were patterned on the ITO-glass substrates by conventional photolithography procedure. Initially, ITO-Glass slides were cleaned by standard glass cleaning process, 5 min sonication in DIW, acetone and 2-propanol in this order. Finally, substrates were dried under N2 flow for 3 minutes. Then, were activated using a plasma cleaner for 20 min at 6.8W (Expanded Plasma Cleaner, PCD-002-CE Model, Harrick Scientific Corporation, NY, USA), and heated at 95º for 1 minutes using a hot plate. AZ1512Hs positive resist (MicroChemical GmbH, Ulm, Germany) was spun on the substrate in two steps, to obtain a final resist thickness of 2 µm (Spinner model WS-650MZ, Laurell Technologies Corporation, North Wales, USA). A soft bake at 95 ºC for 2 min is performed to remove solvents from resist and improve adhesion. IDA pattern was stamp on a Chromium Mask fabricated by direct lithography using a direct write laser machine (DWL) (DWL 66FS model, 405nm, 50mW, Heidelberg Instruments Mikrotechnik GmbH, Heidelberg, Germany). In order to transfer the mask pattern to the resist, the coated substrates were placed under a UV light (λ = 305-450 nm) in the UV photolithography mask aligner (SÜSS Microtec, Germany) at 25 mW cm^{-2} for 5 seconds (125 mJ cm-2). The patterned resist was developed for 1 min using an aqueous solution of the AZ400K Developer (MicroChemicals GmbH, Ulm, Germany) in a 4:1 ratio, afterwards rinsed with distilled water, followed by a hard bake at 120ºC for 1h. Thickness was characterized using profilometer (DEKTAK 6M, Veeco Instruments, NY, USA). Following, a wet etching procedure was performed to etch the ITO not protected by resist. Substrate were submerged in a 6 M solution of a HNO_3/HCl mix and heated at 50ºC by 2 min. Finally, substrates were sonicated for 5min in acetone and IPA, then dry with N_2 flow.

2.8.2. PDMS chip fabrication. Silicon wafer molds were created through a two-layer process using negative photoresist SU8-2100 (MicroChem, Westborough, MA, USA). Microfluidic chip design was printed on a high-quality acetate film to be used as a mask and finally a micro featured master mold was then obtained by contact photolithography. To obtain a Polydimethylsiloxane (PDMS) fluidic chip, a mixture of prepolymer with curing agent (Sylgard 184, Dow corning, Midland, USA) were prepared at a 10:1 ratio, degassed in a vacuum chamber for 1 h, and poured on the SU8 master mold. After overnight incubation at 50 ºC, the PDMS replica was cured, carefully peeled off from the mold, followed by holes punch process. Once PDMS chip was obtained, a bonding step to the ITO-IDA electrode substrate were performed through oxygen plasma activation for 30

s at 10.5 W (Expanded Plasma Cleaner, PCD-002-CE Model, Harrick Scientific Corporation, NY, USA). Then the final microdevice was heated at 80º for 2 h.

2.9. Fabrication of the biosensing platform

2.9.1 Chemical and Immunochemicals. Phosphate-buffered saline (PBS) is phosphate buffer (0.01 M), potassium chloride (0.0027 M) and sodium chloride (0.137 M) at pH 7.2. MES buffer was prepared from MES hydrate salt (4-morpholineethanesulfonic acid) and adjusted to pH 5.0 (M5287, Sigma Aldrich Co. St Louis. MO, USA, respectively). Purified rat anti-mouse IL-6 (ref. 554400, clone MP5-20F3, capture antibody), biotin rat anti-mouse IL-6 (ref. 554402, clone MP5-32C11, detection antibody), purified rat anti-mouse TNF-α (ref. 551225, clone G281-2626, capture antibody), and biotin rat anti-mouse TNF-α (ref. 554415, clone MP6-XT3, detection antibody), were purchased from BD Biosciences (Barcelona, Spain). Recombinant mouse IL-6 (ref. 200-02-100 µg) and recombinant mouse TNF-α (ref. 200-31-100 µg) were purchased from CliniSciences S.L. (Nanterre, France). SAv-polyHRP used in the final step, was purchased from Pierce ThermoFisher (21140, Barcelona, Spain). For electrochemical measurements, it was used citrate buffer (0.04 M, pH 5.5) (S4641, Sigma Aldrich Co. St Louis. MO, USA) and substrate solution was also prepared containing TMB (0.0001%) (3.3',5,5'-tetramethylbenzidine) and H2O2 (0.0004 %) in citrate buffer.

2.9.2. Functionalization protocol. To capture specifically the IL-6 and TNF-α secreted it was necessary to functionalize firstly the surface of SPGEs sensors by using a Self-Assembled monolayer (SAM). To create a uniform SAM, it was used (20-11-Mercaptoundecanoyl)-3,6,9,12,18-hexaoxaeicosanoicacid (TH003-m11.n3-0.5, Prochimia Surfaces, Sopot, Poland). Firstly, the gold SPGE sensors were cleaned using an UV/Ozone cleaner (ProCleanerTM, BioForce Nanosciences, Utah, USA) for 15min. Afterwards, an ethanolic solution of SH-PEG-acid (5 mM) was prepared freshly using 99.5% EtOH HPLC grade (161086.1211, PanReac AppliChem, Barcelona, Spain). The SAM formation step was made in static conditions using a PMMA static cell especially designed for this step (Figure S3b). The SPGE sensors was coupled with PMMA cells and 50 µL of the SH-PEG acid molecule was added in each individual reservoir and left overnight at RT. After SAM formation, electrodes were rinsed in EtOH. In order to facilitate the linkage of protein, it was used carbodiimide chemistry utilizing EDC (200 mM) (E7750, Sigma Aldrich Co. St Louis. MO, USA) mixed 1:1 of N-hydroxysulfosuccinimide sodium salt (sNHS) (200 mM) in H2O (56485, Sigma Aldrich Co. St Louis. MO, USA) and MES buffer (M5287, Sigma Aldrich Co. St Louis. MO, USA) respectively. Once activation is performed, of capture antibody (100 µL) in PBS buffer was added and incubated for 2h at RT. Afterwards, two washes with PBS (10 mM) are performed and electrodes are passivated using PBS (10mM, 1% BSA) for 1 h at RT, to avoid non-specific binding. SPGE electrodes is implanted under microfluidics conditions throughout all the experiment. As final step, SPGE electrodes is removed and placed into static PMMA cell to be processed. At this point, binding of secondary biotinylated antibody was performed, followed by addition of SAv-polyHRP, both steps for 1 h at RT. Finally, SPGE electrodes are connected to potentiostat and amperometric signal recorded. Electrical stimulation was performed using a wave generator (200MHz Multifunction Generator, WF19478, NF Corporation, Yokohama, Japan) connected to microdevice using metallic connections assembled to it. To evaluate accuracy in our experiments, blind spiked samples were prepared in DM and measured directly by our optimized immunoassays. Accuracy for both immunoassays were evaluated by establishing a linear regression between spiked and measured values. Analyses were made by triplicate.

2.9.3. Amperometric detection measurements. Amperometric measurements were performed with a µSTAT 200 potentiostat (Metrohm-Dropsens, Herisau, Switzerland). Screen-printed gold electrodes (SPGE) (Au DRP-220AT, Metrohm-Dropsens, Herisau, Switzerland) consisting of a 4-mm smooth working electrode, an Au counter electrode and a Ag pseudo-reference electrode, were used. A flow cell (DRP-FLWCL, Metrohm-Dropsens, Herisau, Switzerland) for SPGE was used for experiments under flow conditions together with the microdevice. To integrate both systems, and to control the delivery of the cell medium containing the secreted myokines to SPGEs sensors, we used an 8-way flow and pressure control microfluidics distributor (Part No. 001103, Kinesis, Cambridgeshire, UK). The peristaltic pump used in the experiments, it was coupled with a multi-channel pump-head, allowing 8 independent parallel tubing set up (Model MCP Process, Cole-Parmer GmbH, Wertheim, Germany). The microfluidics tubing used in all process was made in PTFE with 1/16" OD x 1/32" ID (Darwin Microfluidics, Paris, France). Once detection was performed, amperometric signals were measured at an applied potential of -0.20 V vs the Ag pseudo-reference electrode during 250 s. The amperometric signals were acquired in static conditions using the static PMMA cell. The recorded signal was the mean value of the current obtained in the last 10s when the steady-state was reached. The specific signal produced for the detection of proteins is translated by the difference between the original base of the citrate buffer and the signal obtained when the substrate solution is added. The intensity registered due to this electron transfer, is directly related with the amount of HRP and, consequently, with the concentration of the IL-6/TNF-α of the analyzed sample through calibration curves.[11] Cyclic voltammetry (CV) measurements were carried out after deposition of $[Fe(CN)6]^{3-/4-}$ (50 µL, 5 mM) redox probe solution onto the surface of the modified Au electrode. CV in the range of -0.25 to 0.50 V at scan rate of 100 mV s^{-1} was used to monitor the SAM formation on electrode gold surface.

2.10 Statistical analysis

Statistical analysis was performed using Graph Prism software (GraphPad Software, San Diego, CA, USA). All data collected were presented as the mean ± standard deviation (SD). Continuous variables were analyzed using Kruskal-Wallis rank test. When significant, post hoc tests for continuous variables were performed among groups by the Mann-Whitney test. p values <0.05 were considered statistically significant.

3. Results and discussion

3.1 Description of the integrated platform

In the recently emerged field of organ-on-a-chip is increasingly recognized the need to incorporate biosensing for in-situ monitoring of the status or metabolic behavior of biomimetic organs. In order to fill this gap, we have developed an integrated platform constituted by a custom-made microdevice hosting a SM microtissue, coupled with functionalized SPGEs biosensing system for a high-sensitive detection of secreted factors such as IL-6 and TNF-α.

The cell medium reservoir, containing 20mL of DM cell media (Fig. 1Aa) is connected with a miniaturized device containing the 3D muscle microtissue, forming the "muscle-on-a-chip." The microdevice is formed by a combination of ITO-IDA electrodes substrate with a polydimethylsiloxane (PDMS) microfluidic chip (Fig. 1Ab). On the top of this system, the SM cells embedded in composite hydrogel are patterned by a molding technique and left to grow, fuse and differentiate until 3D aligned muscle fibers are obtained. Inside the microdevice, 3D microtissue is exposed to either electrical stimulation (from ITO-IDA electrodes) or biological stimulation (addition of LPS to DM cell medium).

As a consequence of either form of stimulation, myokines are secreted from the construct to cell medium and are delivered by microfluidic network to a highly sensitive SPGEs amperometric system (Fig. 1Ac). The SPGEs are functionalized with selective monoclonal antibodies before assembly into the microdevice. Finally, the cell medium delivers secreted myokines directly onto SPGEs sensors. This system is optimized to not dilute the sample avoiding further manipulation by the operator. The capture of these analytes (myokines) produces changes in amperometrical signals which are directly related with concentration. Negative pressures are applied to all system using a peristaltic pump. Our custom-designed microfluidic platform fits in a shelf of standard incubators (Fig. 1B).

3.2. Muscle-on-a-chip integrated with on-site multiplexed sensing system for in-situ monitoring of secreted myokines

3.2.1. Muscle-on-a-chip

As a proof-of-concept, we choose a model based on SM tissues, known to be a secretory organ. Our target SM tissue is fabricated inside the microdevice, enabling not only the renewal of nutrients, but also the electrical stimuli to induce tissue contraction. To fabricate the microdevice, we perform photolithography procedure to obtain an array of ITO-IDA with reference electrodes on a glass substrate for tissue electrical stimulation. The dimensions of whole device are 60 x 60 mm. The size of ITO-IDA arrays is 220 x 110 x 0.1 µm height, width, and thickness, respectively. (Fig. S1A†). The miniaturized chip is built in PDMS placed on top of ITO-IDA electrodes (Fig. 2A). The microdevice is designed and fabricated to be use and integrated with biocompatible materials such as gelatin methacryloyl (GelMA), which provide optimal cell environment. This platform presents a high compatibility with standard sterilization protocols. By other side, using microfluidics network provides low-volume consumption (< 1 mL), ensuring good nutrients exchange with the SM microtissue. The microdevice is also integrated with interdigitated electrodes set for the electrical stimulation of the microtissue mimicking an in vitro exercise model (Fig. 2A).

The size of interdigitated electrodes is 50 µm with a gap of 50 µm between electrodes. To simulate the intensity and penetration of electrical field generated by electrodes array, we use COMSOL Multiphysics® software with AC/DC module. As we expected, electrical current is inversely proportional to the size of the gap between electrodes (Fig. S1B†).[12] We conclude that, 50 x 50 x 0.1 µm electrodes dimension represent a good compromise between electrical field cell tolerance and penetration through the microtissue construct.[13] To stimulate the cells, we set the limit of 1 Hz/5V to avoid electrodes overburn.[14]

To design the PDMS microfluidics chip, we use Computer-Aided Design (CAD) software followed by fabrication with soft lithography technique. After fabrication, we covalently bound the PDMS chip on top of ITO-IDA electrodes trough oxygen plasma process (Fig. 2A). The PDMS chip contains two round wells of 10 mm diameter connected with microchannels of 1 mm height and 0.2 mm width each. Both the inlet and the outlet are fixed at 2 mm diameter; the electrical pin connectors are fixed at 4 mm (Fig, S1C†).

To explore characteristics of the device, we perform theoretical simulations using COMSOL Multiphysics® software (Fluid Flow module). We use a stationary physic study of various flow rates (from 10^4 to 10 µL min^{-1}) to study flow behavior within the microchannels. As expected, the flow velocity mirrors the flow rate since the microchannel cross section (Ø = 0.2 mm^2) is fixed (flow rate = cross section x velocity). The negative pressure gradient from the outlet to the inlet is present and is proportional to flow rate (Fig. S1D and E†). To evaluate the flow velocity and dynamics within the microchambers, we included rectangular prisms (grooves) simulating the 3D muscular microtissue. At higher pressure, the fluid escapes towards the wall of the circular chamber where less resistance is encountered compared with the interspace between the grooves (Fig. 2B, zoom). According to our flow-dynamics simulations in Fig. 2B, we choose a 50 µL min^{-1} as a working shear flow where random fluid motion and shear stress is minimized. This velocity represents the experimental condition where both nutrient diffusion (laminar flow) and microtissue stability (liquid pressure) are optimized. This condition is made possible by fabricating a 3D SM microtissue inside our microdevice using tissue engineering techniques.

Once we have optimized the working conditions of our microdevice, we fabricate a 3D microarchitecture of the native SM tissue using photopolymerized GelMA hydrogel. Because GelMA-based hydrogels can be degraded by cells metabolism, thus affecting spatial and physicochemical properties, we add non-biodegradable

methacrylate carboxy methyl cellulose (CMCMA) to obtain a hydrogel composite (Fig. 3A).[8] To characterize the physical and mechanical properties of GelMA and GelMA-CMCMA, we first expose them to UV light (365 nm) for 18, 24, 30, 60, 120 seconds. Energy dosage was directly measured with a wireless power meter inside de UVP crosslinker chamber obtaining energy values of 0.30, 0.37, 0.48, 0.96 and 2.1 J (W.s) for 18, 24, 30, 60 and 120 s respectively. We find that at longer UV light exposure times, the stiffness of both hydrogels increases (from 0.2 to 1.6 kPa, and 0.3 to 3.9 kPa, respectively, Fig. 3B), but GelMA-CMCMA showed significantly higher compression modulus compared with GelMA alone, in particular after 30 seconds of exposure. As expected, we found that the swelling ratio is inversely correlated with stiffness (Fig. 3B). This can be explained by the fact that the longer UV exposition led to an increase in hydrogel crosslink and decrease in porous size and water uptake. The magnitude of the change in H_2O uptake is higher in GelMA-CMCMA compared with GelMA alone (from 283 to 58 and from 46 to 18, respectively) (Fig. 3B). Moreover, the presence of CMCMA makes the hydrogel more resistant to the enzymatic degradation compared with hydrogel without CMCMA (Fig. 3C). From these evidences, we chose GelMA-CMCMA both for its stability (high stiffness and low enzymatic degradation) and for improved water absorption property (high swelling ratio). The composite hydrogel used to recreate the 3D structure shows a stiffness range between 1 and 3 kPa, which is known to enhance C2C12 3D differentiation.[15] The addition of CMCMA to the hydrogel amplified either stiffness and water absorption (high swelling ratio) which are important factors in cell differentiation and nutrient diffusion inside the polymer (Fig. 3B). Moreover, CMCMA increased the enzymatic degradation resistance, which has a significant impact on experimental variability.

To build the encapsulated 3D SM microtissue inside the composite hydrogel, we use photo-mold patterning technique. This approach presents numerous advantages such as cost-effectiveness, non-surface dependence, and allows fine control over cell alignment, elongation and maturation without any external stimuli, *e.g*. mechanical stretch. First, we use a SU-8 mold, fabricated by photolithography process, to shape PDMS stamp. Second, cell laden hydrogel was micropattern with the PDMS stamp by UV light exposure (Fig. 4A). We incubate the formed 3D SM microtissue in cell medium for 6 days to allow the cells to adapt to the new settings and stimulate further propagation. At this point, the growth medium (10% fetal bovine serum) is replaced with differentiation medium (2% horse serum).

As expected, we observe viable cells throughout the microstructure at 24 seconds of UV exposure at 1, 6 and 10 days of culture compared with 60 seconds (96 ± 3, 87 ± 6, 92 ± 4% and 80 ± 9, 83 ± 7, 86 ± 7% respectively (Figure S2B†). Moreover, UV light exposure time of 24 seconds presents the best cell morphology score, defined by the high aspect ratio (2,149 ± 0,970) a low circularity (0,366 ± 0,188) (Fig. 4B). Therefore, we fixed 24 seconds as the optimal exposure time for the subsequent experiments. Using bright-field microscopy, we observe homogeneous distribution of the cells at day 1 (24h post fabrication) (Fig. 4C). Progressive cell alignment and elongation towards myotube formation is visible at day 10 (black dash lines and arrows, Fig. 4C).

To assess the cell differentiation and maturation, we stain cells with F-actin and myosin heavy chain (MHC), respectively. F-actin stain shows cell elongation and alignment at day 10 throughout the entire thickness of the 3D muscle microtissue compared with random myotube distribution in the non-patterned control group (Fig. 5A). We found that the 3D microgrooves restrict the degree of cell alignment between 0° and 15°, whereas the non-patterned cells are randomly distributed showing cell alignment ranging from 0°-90° (Fig. 5B). Furthermore, 3D muscle microtissue enhances myotube maturation and cell fusion compared with three-dimensional non-patterned cells assessed by MHC staining and fusion index, respectively (75 ± 7 vs 50 ± 3 $p < 0.001$, Fig. 5C). We note that, the exposure of the microstructure to UV light for 24 seconds enables precise control of cellular organization in 3D and promotes cell myogenic differentiation and maturation. This in vivo-like structure enhances cell organization with a positive impact on cell viability and function up to 10 days of culture. Longer UV light exposure increases the stiffness of GelMA-CMCMA reducing cell spatial organization, but not affect the viability (Fig. S2A†). The control of the hydrogel microgeometry (microgrooves) is the main factor that improves cell maturation and alignment, pushing engineered tissue one step closer towards the creation of functional in vitro tissue.[16]

3.2.2. On-site multiplexed sensing system

After fabrication and characterization, the muscle-on-a-chip is connected to a high-sensitive cytokines biosensing system (Fig. 6A and B) to monitor the release of myokines. In this work, the medium flow coming from the 3D SM tissue pass through the on-site multiplexed sensing system (Fig. 1B number 5). The commercial SPGEs, where we previously immobilized antibodies against IL-6 and TNF-α, bind the cytokines present in the medium. Once binding is performed, SPGEs electrodes were finally located in the static PMMA cell, and secondary antibody and enzymatic tracer was added. The enzymatic reaction produces changes in the electrode current density on the surface that are directly related with the amount of cytokines detected by primary antibody.

For signal transduction, we chose commercial SPGEs because of their numerous advantages such as favorable electron transfer kinetics, good stability, and convenient covalent bonding with functional groups such as thiol-containing molecules (through the formation of gold (Au)-SH bonds). For detection of secreted myokines in cell medium, the surface of SPGEs was used to anchor IL-6 and TNF-α antibodies. To assess the full coverage of SPGEs surface by the SAM we used cyclic voltammogram technique.[17] Briefly, bare electrode (no SAM layer) showed the typical voltammogram characterized by a cathodic and anodic current peaks for a reversible reaction (dash line in Fig. S3A†) whereas when the SPGEs surface with a monolayer of SH-PEG-acid a decrease in the current is observed due to the blocking properties of the monolayer (blue curve in Fig. S3A†).

The SH-PEG-acid is activated using the EDC/NHS reaction followed by the covalent immobilization of primary IL-6 and TNF-α antibodies. To detect cell secreted myokines, we use a sandwich

immunoassay that involves exposure to biotinylated primary antibodies followed by streptavidin-horse radish peroxidase (HRP) complex (SAv-polyHRP). The HRP-catalyzed 3,3',5,5'-tetramethylbenzidine (TMB) reaction is recorded via amperometric signal (Fig. 6A). The on-site multiplexed sensing system for each cytokine is constituted by 5 parts: 1) poly methyl methacrylate (PMMA) microfluidic cell cover; 2) SPGE functionalized electrodes; 3) stainless steel electrodes support case; 4) cell detection chamber coupled with microfluidic connectors; 5) potentiostat (Fig. 6B). Before connecting this sensing system to the muscle-on-a-chip through an 8-way flow distributor, we optimized the immunoassay parameters one by one.

First, we performed enzyme-linked immunosorbent assays (ELISA) test to validate the two commercial antibodies used in this study. We observed the limit of detection (LOD) 0.031 ± 0.010 ng mL^{-1} with slope of 0.726 ± 0.008 and LOD 0.060 ± 0.020 ng mL^{-1} with slope 0.498 ± 0.012 for IL-6 and TNF-α, respectively (Fig. S3C†). Second, we validated the primary antibody anchorage on SH-PEG-acid/Au surface using a static PMMA case (Fig. S3B†). Here, we observed a saturation plateau at 1.5 and 10 µg mL^{-1} for IL-6 and TNF-α, respectively (Fig. S3D†). Third, the optimal concentration of secondary biotinylated antibody found were 5 and 40 µg mL^{-1} for IL-6 and TNF-α, respectively (Fig. S3E†). Fig. S3F† shows the optimal attachment kinetics of the SAv-polyHRP to the secondary at 1 µg mL^{-1} for both systems. We set at 160 seconds the time of HRP-catalyzed TMB oxidation. Finally, these optimized values were used in later determination of calibrations curves, which represent the working conditions to obtained lowest LOD. Calibration curves under fluidic condition, showed a LOD of ~8 ng mL^{-1} and ~2 ng mL^{-1} with effective concentration 50 (EC50) of ~78 ng mL^{-1} and ~20 ng mL^{-1} for IL-6 and TNF-α, respectively, with no matrix effect and high signal/noise ratio (Fig. 6C and D). Moreover, four-parameter logistic regression of the data showed slopes, R^2 of 0.92 ± 0.39 (mean ± SD), 0.8386 for IL-6 and 1.04 ± 0.31 and 0.9497 for TNF-α. Previous experiments demonstrated no cross reactivity between IL-6 and TNF-α (data not shown). Both assays showed a satisfactory accuracy (slope close to 1, Fig. S3G†).

To note, few examples can be found in literature that incorporate microfluidic platform with biosensing system to study the metabolism of various tissues.[4, 5] For instance, the use of a non-label transduction like in the case of the impedance allows simple acquisition; however, without enzymatic amplification is less robust regarding changes in medium composition, especially with high ionic buffers. On the other hand, magnetic particles offer an easy system to regenerate the sensors; but the number of possible acquisitions is reduced only daily measurements can be performed, which is not informative enough for metabolic studies. The transduction system used in this study was not affected by any medium under investigation and successfully employed as *in vitro* model of exercise where electrical stimulation with several measures per hour needed.

3.3. In situ monitoring of secreted myokines upon electrical and biological stimulation

For the final part of this study, the microdevice, the 3D muscle microtissue, and the on-site multiplexed sensing system are assembled through a microfluidic network to measure the release of factors upon electrical and biological stimulation.

SM tissues have been identified as an endocrine organ that produces and releases cytokines, which have been named myokines.[18] These compounds such as IL-6 and TNF-α play important roles in biological processes such as energy metabolism, angiogenesis, myogenesis, and muscle repair.[19-22]

The system is assembled trough microfluidic network as you can see in Fig. 1A and B. The flow pass through the chip where 3D SM tissue is electrically or biologically stimulated. The outlet flow goes directly to an 8-way microfluidic distributor to reach the SPGEs sensing system. A peristaltic pump generates negative pressures that pull medium to SPGEs. After binding SPGEs are removed and processed separately.

The focal points of this work are the investigation of source and secretion regime of IL-6 and TNF-α either in muscle stress or during inflammatory process. Firstly, to find the most responsive biological stimulus for IL-6 and TNF-α secretion, 2D monolayers of differentiated myotubes were incubated in cell culture plates with Caffeine, Dexamethasone and LPS.[23-25] After determine cytokine secretion levels by ELISA, LPS, over caffeine and dexamethasone, showed the highest release of IL-6 in the medium whereas similar values among the conditions were obtained with TNF-α release (Fig. S4A†). TNF-α values do not show significant changes under all the treatments (Fig. S4B†). According with these results LPS was used as biological agent to induce cytokines release in our integrated sensing system.

We performed continual electrical stimulation using a wave generator connected with muscle-on-a-chip through electrical pins, operating at 5V (peak-peak), at a frequency of 1 Hz with a width of 2 ms for 60 min. We measured the release of myokines every 15 min (switching the 8-way flow distributor) during 1 hour of stimulation phase followed by 1 hour of relaxation phase (*i.e.*, without stimulation). The control group did not receive any electrical stimulation. Fig 7 show, the monitoring of IL-6 and TNF-α concentrations at each period of time, for both stimulation regimes. With this fast acquisition system, we detected up to 1 µg mL^{-1} for IL-6 and 10 ng mL^{-1} for TNF-α in DM during the relaxation time after electrical stimulus was ended (mimicking exercise training) (Fig. 7A). Fig 7B demonstrates the release of myokines after supplementation of the medium with LPS 10 µg mL^{-1} for 48h. In case of IL-6, the maximum detectable peak is reached within 1 hour of stimulation and then it is maintained almost constant. IL-6 concentrations over 2.5 µg mL^{-1} were detected (~ 3 pg mL^{-1} per cell, calculating using an estimation of 840.000 encapsulated cells per microdevice, Fig. S4C†) after 1 hour of LPS addition. Conversely, we observed a slow but constant increase of TNF-α throughout all the experiment, reaching over 50 ng mL^{-1} (~0.07 pg mL^{-1} per cell, calculating using an estimation of 840.000 encapsulated cells per microdevice, Fig. S4D†) in 48 hours (Fig. 7B).

Here, we have demonstrated that secretion of these cytokines in SM is regulated by exercise stress. The study of SM metabolism lies in the timing of release of those factors, which take place 15 minutes after the end of electrical stimulation. These experiments suggest that SM cells might play a potential role in the myogenic process. Even more interesting is the quicker and higher release of these factors from cells as consequence of LPS stimulation compared with electrical stimulus only (~2 times for IL-6 and TNF-α at 1 hour of stimulation) (Fig. 7B). These evidences might reshape the role of SM cells in response of bacterial toxins. As such, the development of this novel technology applied to this particular system, represents a further and important step for development of biomimetic muscle platforms to monitor skeletal muscle cytokine functions for quantitative exploration of inflammatory and regenerative process, strongly interconnected with myopathy disease. Nevertheless, promising applications in other organs systems (individually or combination or various) are open, to best understand biological mechanisms needed of a continual in situ monitoring of secreted factors.

Besides, IL-6 and TNF-α are pleiotropic cytokines with a multiple effect on immune and non-immune cells. Among those effects, these myokines can play an important role in regulating protein and glucose metabolism during tissue injury. In case of SM cells these soluble factors are fast way of communication between the cells of the same organ, but also between different organ. This platform can help us to understand the magnitude and the timing of response upon different chemical and physical stimuli in order to identify a window for therapy.

4. Conclusions

We have developed an innovative cost-effective platform capable of simultaneous, in-situ cell stimulation and analytes over time detection. Our custom-made microdevice was fabricated and used to host a mature and highly aligned SM tissue obtained using GelMA-CMCMA hydrogels. This 3D in vivo-like tissue, known to release cytokines under external stimulations, was combined either with a highly controlled flow platform, which provide electrical stimulation using ITO-IDA electrodes or biological stimulation supplementing cell medium with LPS, together with a high-sensitive in-situ sensing system. We functionalized our sensing system with the purpose of achieve a multiplexed continual in-situ measurements of secreted myokines. This unique approach allowed us to detect the release of two important cytokines such as IL-6 and TNF-α from 3D muscle tissue. We conclude that skeletal muscle cells can express and release these factors in response to electrical stimuli and LPS administration. We are currently working on optimizing this platform for in depth investigation of myogenic process and inflammatory response. This revolutionary technology can be exported to any laboratory environment and can have a huge impact on drug-screening process.

Conflicts of interest

There are no conflicts to declare.

Author contributions

M.A.O, X.F, A.G.C, A.H and J.R. conceived and planned the experiments. X.F and A.G.C carried out biological experiments related with 3D SM tissue formation and characterization. M.A.O, A.H, J.B developed the sensing platform. M.A.O, J.B, performed integrated experiments and acquisition of data. M.A.O, A.G.G, A.H and J.R contributed to the interpretation of the results. F.DC and M.A.O drafted and edited the manuscript. J.R supervised the project. All authors provided critical feedback and helped shape the research, analysis and manuscript.

Acknowledgements

Funding for this project was provided by the Ramon y Cajal (RYC-2014-15022) fellowship and Severo Ochoa Program for Centers of Excellence (R&D 2016- 2019) funded by the Ministerio de Economía, Industria y Competitividad; an ERC grant (ERC starting grant project – 714317 – DAMOC); the CERCA Programme/Generalitat de Catalunya (2014-SGR-1442 and 2014-SGR-1460); and the Fundación Bancaria "la Caixa"-Obra Social "la Caixa" (projecte IBEC-La Caixa Healthy Ageing). Authors wants to thanks to Mr. Xavier Menino Pizarro, Engineering Mechanics Head from Research Technical Support Unit at Institute of Photonics Sciences (ICFO) for the design and fabrication of the custom-made pieces used in this work. Also, we would like to thanks to Dr. Minseong Kim for his drawing skill.

Figure Legends

Fig. 1. Schematic overview of the configuration and function of the muscle-on-a-chip. (A) The flow pass through the microdevice where 3D SM tissue is electrically (ITO-IDA electrodes) or biologically (LPS) stimulated. The outlet flow containing the IL-6 and TNF-α goes directly to an 8-way microfluidic distributor to reach the SPGEs sensing system. A peristaltic pump generates negative pressures that pull the medium trough the microdevice as well as the detection system (SPGEs). a) reservoir containing cell media connected with a b) custom-made microdevice containing the 3D SM tissue. c) multiplexed high-sensitive platform containing functionalized SPGEs. (B) Physical arrangement: 1) cell medium reservoir; 2) 3D engineered muscle microtissue cultured on the microdevice; 3) microdevice support; 4) 8-way flow distributor; 5) SPGEs functionalized sensing system.

Fig. 2. Designing and fabrication of microdevice. (A) Schematic image shows the assembling elements and microdevice. (B) COMSOL Multiphysics® simulation of Flow velocity and dynamic through microfluidic network. Various simulations were

performed ranging from to 10^4 to 1 µL min^{-1} velocities. Black lines inside the chamber represent the 3D muscle microtissue.

Fig. 3. (A) Gelatin methacryloyl (GelMA) and Carboxymethyl cellulose methacrylate (CMCMA) chemical structures. (B) mechanical characterization of composite hydrogel GelMA-CMCMA and comparison with only GelMA. (C) Matrix degradation study of GelMA and GelMA-CMCMA hydrogel exposed at different UV times. Data from three different experiments (mean, SD): **p<0.01; ***p<0.001

Fig. 4. Fabrication and characterization of 3D muscle microtissue. (A) Schematic view of the photo-mold patterning technique used to fabricate the skeletal muscle microtissue. (B) Cell morphology evaluation (Circularity and Aspect ratio) at different UV exposure times. (C) Bright-field characterization of skeletal muscle cells embedded in 3D composite hydrogel. Dashed lines at 10 days indicate muscular fibers. Black arrows at day 6 and 10 indicate the microtubule formation. Scale bars: 200, 100 and 50 µm; top, middle and bottom panel respectively.

Fig. 5. (A) Immunostaining for 3D Skeletal muscle microtissue for non-patterned (control) and microstructured hydrogel evaluated by phalloidin (red) staining. Cell differentiation was assessed by MHC staining (green). Nuclei were stained by DAPI. Scale bars: 200 µm (B) and (C) Cell orientation and fusion index characterization for non-patterned vs microstructured 3D skeletal muscle tissue. Data from three different experiments (mean, SD): *p < 0.05, **p < 0.01; ***p < 0.001.

Fig. 6. On-site multiplexed sensing system description and characterization. (A) Schematic representation of steps for sandwich immunoassay as detection mechanism. (B) Biosensing system physical arrangement: 1) PMMA microfluidic cell cover; 2) SPGEs functionalized electrode; 3) Stainless steel electrodes support case; 4) Cell detection chamber coupled with microfluidic connectors; 5) Potentiostat. (C) Raw amperometric signals and calibration curves performed in differentiation media and under fluidic condition for IL-6 and TNF-α. Curves shown limits of detection of 8 ng mL^{-1} and 2 ng mL^{-1} for IL-6 and TNF-α, respectively.

Fig. 7. IL-6 and TNF-α detection by in situ- monitoring upon either (A) electrical stimulation (cycle 5 V/1 Hz for 105 min, with a 15 min interval) or (B) LPS-stimulation (10 µg mL^{-1}) for 48 hours of 3D cultured skeletal muscle cell.

References

1. A. Khademhosseini, R. Langer, J. Borenstein and J. P. Vacanti, *Proceedings of the National Academy of Sciences of the United States of America*, 2006, **103**, 2480-2487.

2. M.-H. Wu, S.-B. Huang and G.-B. Lee, *Lab on a Chip*, 2010, **10**, 939-956.

3. W. Bian and N. Bursac, *IEEE engineering in medicine and biology magazine : the quarterly magazine of the Engineering in Medicine & Biology Society*, 2008, **27**, 109-113.

4. A. Skardal, S. V. Murphy, M. Devarasetty, I. Mead, H.-W. Kang, Y.-J. Seol, Y. Shrike Zhang, S.-R. Shin, L. Zhao, J. Aleman, A. R. Hall, T. D. Shupe, A. Kleensang, M. R. Dokmeci, S. Jin Lee, J. D. Jackson, J. J. Yoo, T. Hartung, A. Khademhosseini, S. Soker, C. E. Bishop and A. Atala, *Scientific reports*, 2017, **7**, 8837.

5. Y. S. Zhang, J. Aleman, S. R. Shin, T. Kilic, D. Kim, S. A. Mousavi Shaegh, S. Massa, R. Riahi, S. Chae, N. Hu, H. Avci, W. Zhang, A. Silvestri, A. Sanati Nezhad, A. Manbohi, F. De Ferrari, A. Polini, G. Calzone, N. Shaikh, P. Alerasool, E. Budina, J. Kang, N. Bhise, J. Ribas, A. Pourmand, A. Skardal, T. Shupe, C. E. Bishop, M. R. Dokmeci, A. Atala and A. Khademhosseini, *Proc Natl Acad Sci U S A*, 2017, **114**, E2293-E2302.

6. A. Grosberg, P. W. Alford, M. L. McCain and K. K. Parker, *Lab on a Chip*, 2011, **11**, 4165-4173.

7. R. Riahi, S. A. M. Shaegh, M. Ghaderi, Y. S. Zhang, S. R. Shin, J. Aleman, S. Massa, D. Kim, M. R. Dokmeci and A. Khademhosseini, *Scientific reports*, 2016, **6**, 24598.

8. A. García-Lizarribar, X. Fernández-Garibay, F. Velasco-Mallorquí, A. G. Castaño, J. Samitier and J. Ramon-Azcon, *Macromolecular Bioscience*, 2018, **18**, 1800167.

9. M. L. Oyen, *International Materials Reviews*, 2014, **59**, 44-59.

10. P. Occhetta, N. Sadr, F. Piraino, A. Redaelli, M. Moretti and M. Rasponi, *Biofabrication*, 2013, **5**, 035002.

11. P. Fanjul-Bolado, M. B. González-García and A. Costa-García, *Anal Bioanal Chem*, 2005, **382**, 297-302.

12. P. Van Gerwen, W. Laureyn, W. Laureys, G. Huyberechts, M. Op De Beeck, K. Baert, J. Suls, W. Sansen, P. Jacobs, L. Hermans and R. Mertens, *Sensors and Actuators B: Chemical*, 1998, **49**, 73-80.

13. S. Ahadian, J. Ramón-Azcón, S. Ostrovidov, G. Camci-Unal, V. Hosseini, H. Kaji, K. Ino, H. Shiku, A. Khademhosseini and T. Matsue, *Lab on a Chip*, 2012, **12**, 3491-3503.

14. I. J. A. Evers-van Gogh, S. Alex, R. Stienstra, A. B. Brenkman, S. Kersten and E. Kalkhoven, *Scientific reports*, 2015, **5**, 10944.

15. M. Costantini, S. Testa, P. Mozetic, A. Barbetta, C. Fuoco, E. Fornetti, F. Tamiro, S. Bernardini, J. Jaroszewicz, W. Swieszkowski, M. Trombetta, L. Castagnoli, D. Seliktar, P. Garstecki, G. Cesareni, S. Cannata, A. Rainer and C. Gargioli, *Biomaterials*, 2017, **131**, 98-110.

16. V. Hosseini, S. Ahadian, S. Ostrovidov, G. Camci-Unal, S. Chen, H. Kaji, M. Ramalingam and A. Khademhosseini, *Tissue engineering. Part A*, 2012, **18**, 2453-2465.

17. S. Campuzano, M. Pedrero, C. Montemayor, E. Fatás and J. M. Pingarrón, *Journal of Electroanalytical Chemistry*, 2006, **586**, 112-121.

18. B. K. Pedersen and M. A. Febbraio, *Physiological reviews*, 2008, **88**, 1379-1406.

19. J. Li, N. C. King and L. I. Sinoway, *Journal of applied physiology (Bethesda, Md. : 1985)*, 2003, **95**, 577-583.

20. P. Munoz-Canoves, C. Scheele, B. K. Pedersen and A. L. Serrano, *The FEBS journal*, 2013, **280**, 4131-4148.

21. M. Ost, V. Coleman, J. Kasch and S. Klaus, *Free radical biology & medicine*, 2016, **98**, 78-89.

22. J. H. Yoon, J. Kim, P. Song, T. G. Lee, P.-G. Suh and S. H. Ryu, *Advances in Biological Regulation*, 2012, **52**, 340-350.

23. T. Egawa, Y. Ohno, A. Goto, T. Sugiura, Y. Ohira, T. Yoshioka, T. Hayashi and K. Goto, *Journal of Caffeine Research*, 2016, **6**, 88-96.

24. K. Shimizu, R. Genma, Y. Gotou, S. Nagasaka and H. Honda, *Bioengineering (Basel, Switzerland)*, 2017, **4**.

25. R. A. Frost, G. J. Nystrom and C. H. Lang, *American journal of physiology. Regulatory, integrative and comparative physiology*, 2002, **283**, R698-709.

Figure 1

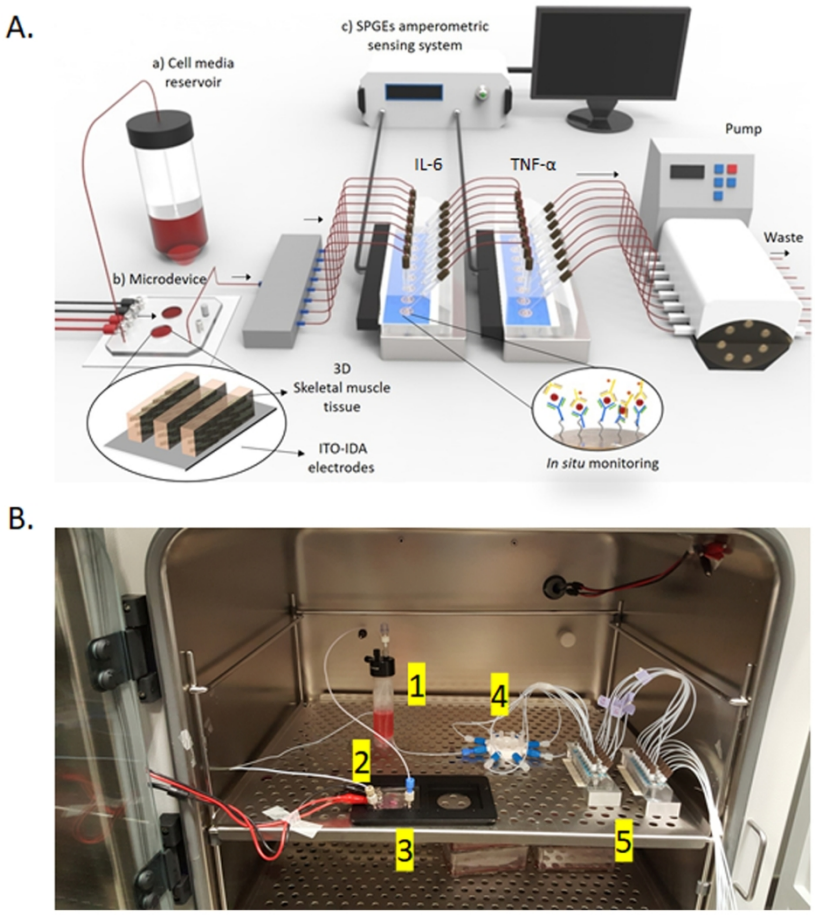

Fig 1. Schematic overview of the configuration and function of the muscle-on-a-chip. (A) The flow pass through the microdevice where 3D SM tissue is electrically (ITO-IDA electrodes) or biologically (LPS) stimulated. The outlet flow containing the IL-6 and TNF-α goes directly to an 8-way microfluidic distributor to reach the SPGEs sensing system. A peristaltic pump generates negative pressures that pull the medium trough the microdevice as well as the detection system (SPGEs). a) reservoir containing cell media connected with a b) custom-made microdevice containing the 3D SM tissue. c) multiplexed high-sensitive platform containing functionalized SPGEs. (B) Physical arrangement: 1) cell medium reservoir; 2) 3D engineered muscle microtissue cultured on the microdevice; 3) microdevice support; 4) 8-way flow distributor; 5) SPGEs functionalized sensing system.

209x230mm (300 x 300 DPI)

Figure 2

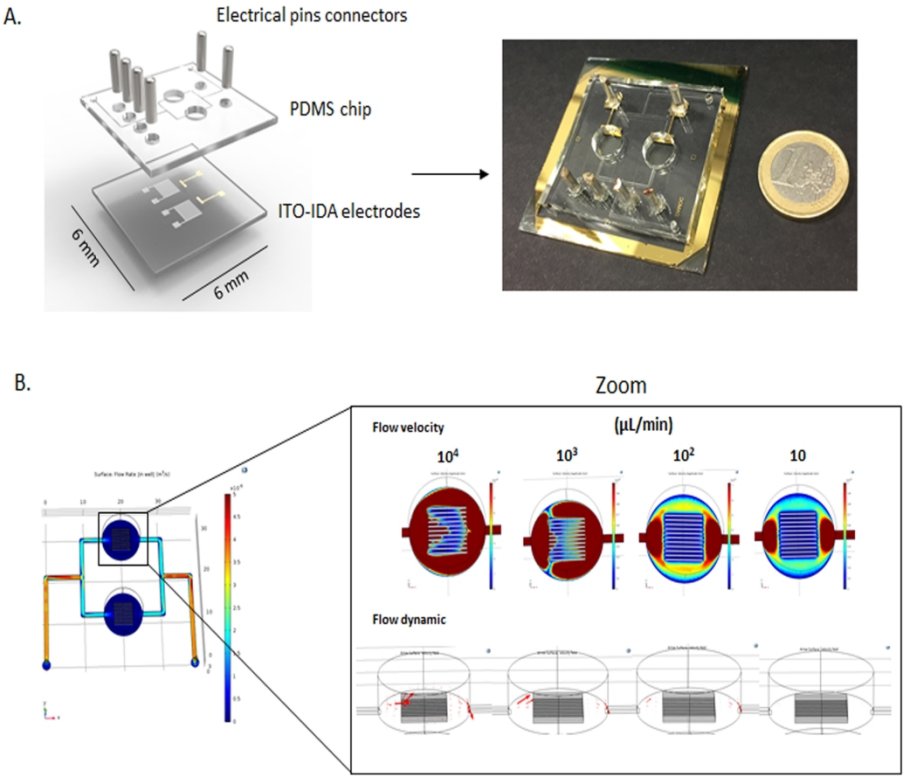

Fig. 2. Designing and fabrication of microdevice. (A) Schematic image shows the assembling elements and microdevice. (B) COMSOL Multiphysics® simulation of Flow velocity and dynamic through microfluidic network. Various simulations were performed ranging from to 104 to 1 µL min-1 velocities. Black lines inside the chamber represent the 3D muscle microtissue.

207x192mm (300 x 300 DPI)

Figure 3

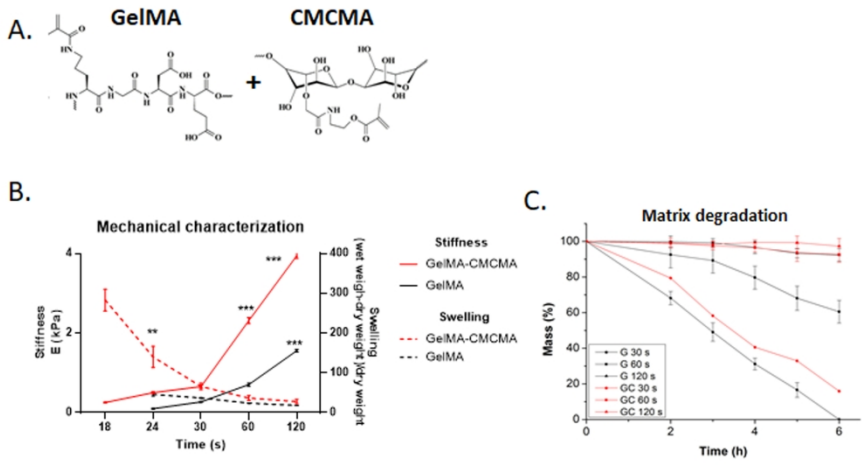

Fig. 3. (A) Gelatin methacryloyl (GelMA) and Carboxymethyl cellulose methacrylate (CMCMA) chemical structures. (B) mechanical characterization of composite hydrogel GelMA-CMCMA and comparison with only GelMA. (C) Matrix degradation study of GelMA and GelMA-CMCMA hydrogel exposed at different UV times. Data from three different experiments (mean, SD): **p<0.01; ***p<0.001

170x111mm (300 x 300 DPI)

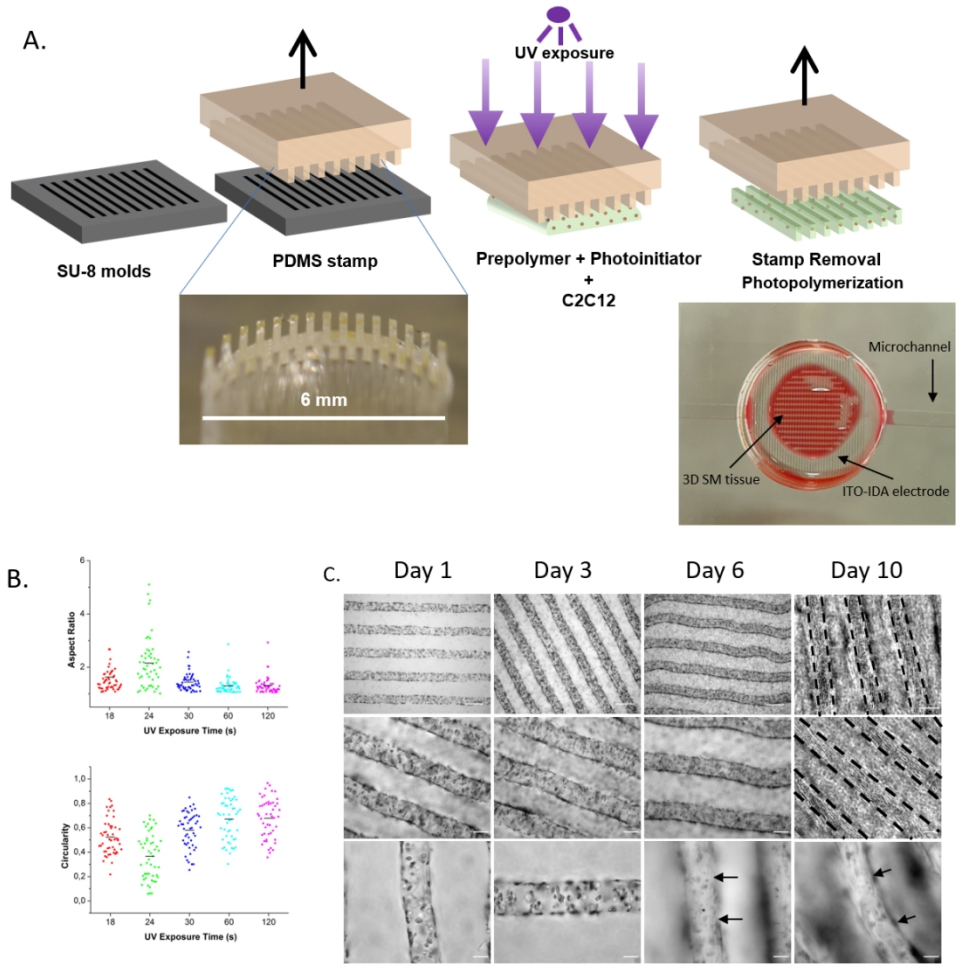

Fig. 4. Fabrication and characterization of 3D muscle microtissue. (A) Schematic view of the photo-mold patterning technique used to fabricate the skeletal muscle microtissue. (B) Cell morphology evaluation (Circularity and Aspect ratio) at different UV exposure times. (C) Bright-field characterization of skeletal muscle cells embedded in 3D composite hydrogel. Dashed lines at 10 days indicate muscular fibers. Black arrows at day 6 and 10 indicate the microtubule formation. Scale bars: 200, 100 and 50 μm; top, middle and bottom panel respectively.

214x212mm (150 x 150 DPI)

Figure 5

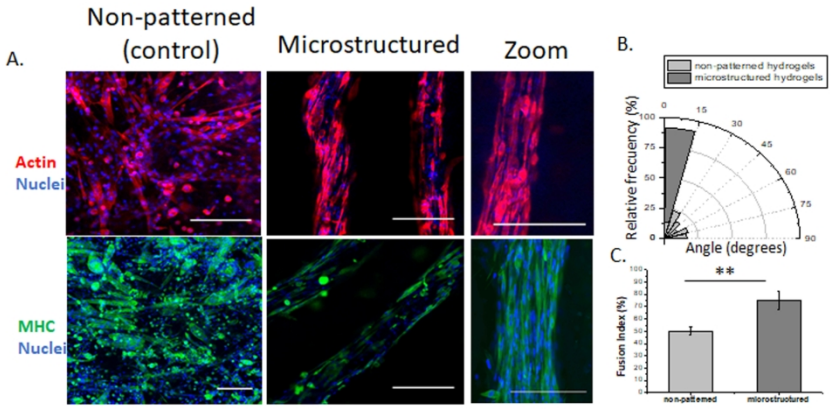

Fig. 5. (A) Immunostaining for 3D Skeletal muscle microtissue for non-patterned (control) and microstructured hydrogel evaluated by phalloidin (red) staining. Cell differentiation was assessed by MHC staining (green). Nuclei were stained by DAPI. Scale bars: 200 μm (B) and (C) Cell orientation and fusion index characterization for non-patterned vs microstructured 3D skeletal muscle tissue. Data from three different experiments (mean, SD): *p < 0.05, **p < 0.01; ***p < 0.001.

189x113mm (300 x 300 DPI)

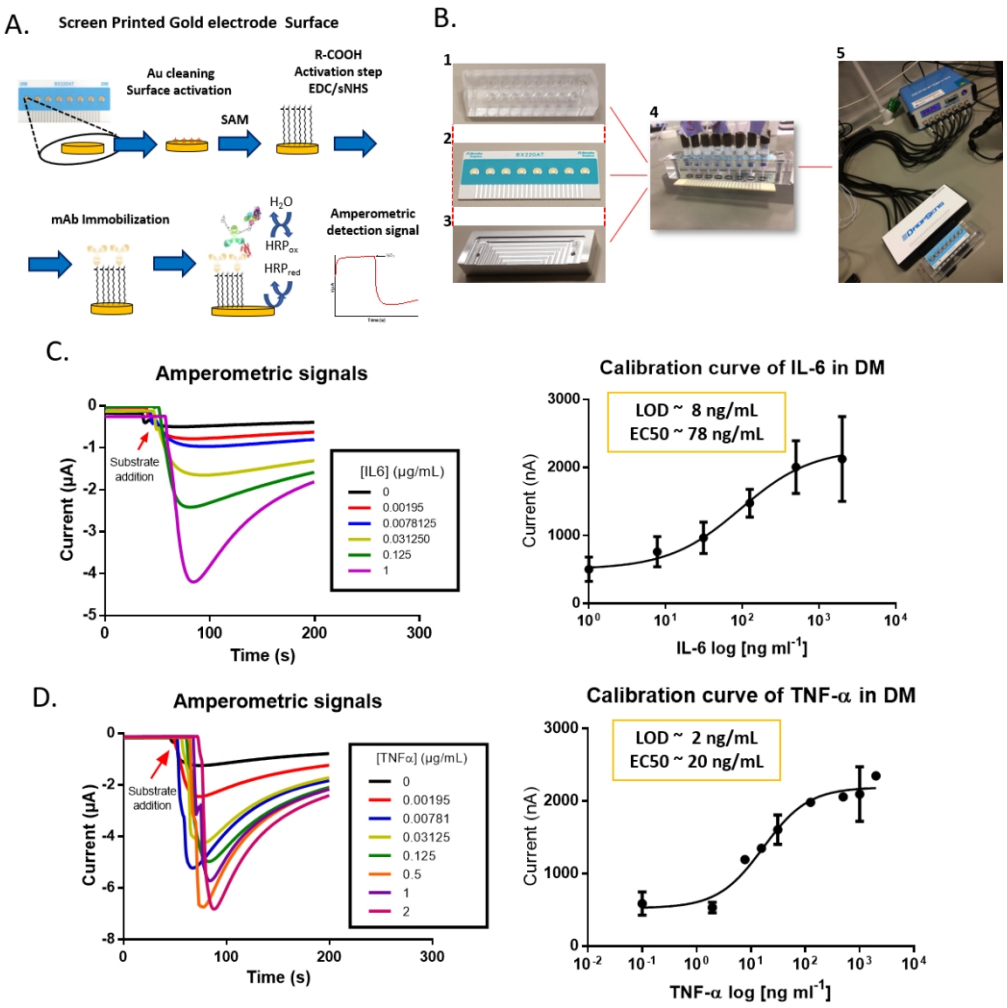

Fig. 6. On-site multiplexed sensing system description and characterization. (A) Schematic representation of steps for sandwich immunoassay as detection mechanism. (B) Biosensing system physical arrangement: 1) PMMA microfluidic cell cover; 2) SPGEs functionalized electrode; 3) Stainless steel electrodes support case; 4) Cell detection chamber coupled with microfluidic connectors; 5) Potentiostat. (C) Raw amperometric signals and calibration curves performed in differentiation media and under fluidic condition for IL-6 and TNF-α. Curves shown limits of detection of 8 ng mL-1 and 2 ng mL-1 for IL-6 and TNF-α, respectively.

Figure 7

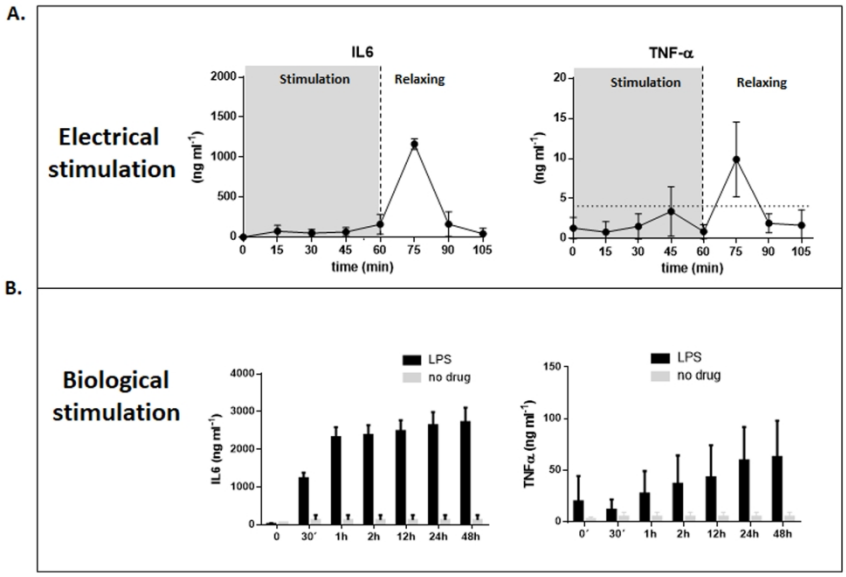

Fig. 7. IL-6 and TNF-α detection by in situ- monitoring upon either (A) electrical stimulation (cycle 5 V/1 Hz for 105 min, with a 15 min interval) or (B) LPS-stimulation (10 µg mL-1) for 48 hours of 3D cultured skeletal muscle cell.

195x137mm (300 x 300 DPI)